AIAA 94-3137

Near and Far-field Plume Studies of a 1 kW Arcjet

Alec D. Gallimore, Sang-Wook Kim, John E. Foster,
Lyon B. King, and Frank S. Gulczinski III

Plasma-physics and Electric Propulsion Laboratory
Department of Aerospace Engineering
The University of Michigan
Ann Arbor, MI

30th AIAA/ASME/SAE/ASEE Joint Propulsion Conference
June 27-29, 1994 / Indianapolis, IN

For permission to copy or republish, contact the American Institute of Aeronautics and Astronautics
370 L'Enfant Promenade, S.W., Washington, D.C. 20024

Near and Far-field Plume Studies of a 1 kW Arcjet

Alec D. Gallimore*, Sang-Wook Kim,†John E. Foster,† Lyon B. King,†
and Frank S. Gulczinski III†
Plasma-physics and Electric Propulsion Laboratory
Department of Aerospace Engineering
The University of Michigan
Ann Arbor, MI USA 48109-2118

June 28, 1994

Abstract

In order to begin the process of characterizing transport in arcjet plumes, profiles of electron temperature, number density, pressure, and flow field patterns were obtained over an extensive volume of the plume of a 1 kW arcjet operating on hydrogen. Axial and radial measurements made over a region of the plume that extends from the arcjet exit plane to over one meter downstream of it are reported. Emission spectroscopy measurements of electron temperature were made near the exit plane of the arcjet. All experiments were performed in a 6 m by 9 m vacuum chamber with a pumping speed of over 100,000 l/s on hydrogen. Tank pressure was typically maintained to less than 3.8×10^{-4} Torr during arcjet operation. In addition to the plume study, arcjet performance measurements are reported.

Nomenclature

A	= probe surface area, m^2
A_e	= nozzle exit area, m^2
A^*	= nozzle throat area, m^2
e	= elementary charge, 1.6×10^{-19} C
g	= gravitational constant, 9.81 m/s^2
I_{sp}	= specific impulse, sec
i_+	= dimensionless ion saturation current
I_+	= ion saturation current, A
k	= Boltzmann's constant, 1.38×10^{-23} J/K
m_e	= electron mass, 9.11×10^{-31} kg
M_i	= ion mass, kg
$\dot{m}$	= propellant mass flow rate, kg/s
n_e	= electron number density, m^{-3}
P	= plume pressure, Pa
P_a	= thruster power, W
q	= dynamic pressure, Pa
r_e	= nozzle exit radius, m
r	= radius from plume centerline, m
r_p	= Langmuir probe collector electrode diameter, cm
kT_e	= electron temperature, eV
V	= probe bias, V
Z_i	= ion charge
η_{th}	= thrust efficiency
γ	= ratio.of specific heats
λ_D	= Debye length, cm
λ_e	= electron mean free path, cm
λ_i	= ion mean free path, cm
Φ_p	= plasma potential, V
χ_p	= dimensionless probe potential
θ	= flow angle

*Assistant Professor, Member AIAA
†Graduate Assistant, Member AIAA

Introduction

Arcjets currently enjoy a high degree of success having been qualified and used for North-South station-keeping duties on the Martin Marietta Astro Space Series 7000 communication satellite[1]. A number of technical issues still remain to be resolved, however, if the full potential of these engines is to be realized. This is particularly true for the higher powered arcjets that are proposed for orbit transfer and orbit maneuvering applications[2, 3, 4, 5, 6]. These issues include understanding how input power is parceled among the various energy modes of the working fluid as well as how it is deposited into the arcjet structure (e.g., electrode losses), and how the transport of mass, momentum, and energy in the plume may affect spacecraft operation and lifetime.

In order to begin the process of characterizing transport in arcjet plumes, profiles of electron temperature, number density, pressure, and the flow field were obtained over an extensive volume of a 1 kW arcjet plume. Axial and radial profile measurements were made with pressure probes and Langmuir probes over a region of

Copyright © 1994 by the American Institute of Aeronautics and Astronautics, Inc.
All rights reserved.

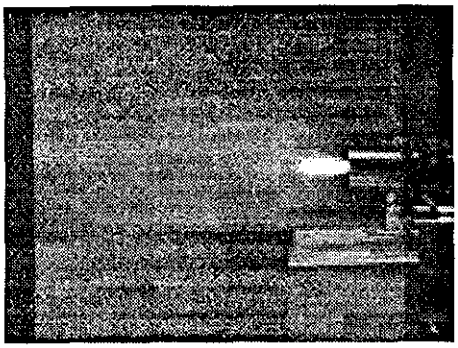

Figure 1: 1 kW Arcjet in operation.

the plume that extends from the arcjet exit plane to over one meter downstream of it. This work extends prior work[7, 8] by comparing the results of of Langmuir probes of different sizes, by providing more of a characterization of the flow-field, and by making detailed pressure profile measurements.

The arcjet was operated on simulated hydrazine, ammonia, and pure hydrogen. Because of space and time limitations, only results with pure hydrogen are reported. In addition to the plume study, arcjet performance measurements were made as well and are reported. It is hoped and anticipated that knowledge gained from this work can be applied to higher powered devices for a variety of propellants.

Experimental Apparatus

A 1 kW-class arcjet that was supplied by the NASA Lewis Research Center (LeRC) was used for this study (cf. Fig. 1). The engine features a 2%-thoriated tungsten cathode and a nozzle (also of 2%-thoriated tungsten) that serves as the anode. The arcjet has a 0.51-mm-diameter by 0.25-mm-long constrictor, a 30 degree half-angle converging nozzle section upstream of the constrictor, and a 20 degree half-angle diverging section. The exit diameter of the nozzle is 9.52 mm, giving the expansion section an area ratio of 350. The electrode gap spacing is 0.51 mm. The outer housing of the device is constructed of titaniated zirconiated molybdenum (TZM).

Arcjet power is provided by a 1800 Watt Sorenson power supply that is conditioned by a NASA Lewis Power Processing Unit (PPU). The PPU nominally operates at output voltages of between 100 and 120 Volts and at currents between 6 and 12 A with ± 1.5 A ripple[9].

Arcjet voltage is measured with Tektronix P6007 100:1 voltage probes clamped to the electrode leads. The voltage probe signals are collected by a Tektronix AM501 operation amplifier. Digital multimeters are used to measure the discharge voltage as well. Arcjet current is monitored with a Tektronix A6303 current sensor powered by a Tektronix AM503 current probe amplifier. Arcjet voltage and current data are monitored and stored by the computerized data acquisition system described below.

All experiments reported were performed in a 9-m-long by 6-m-diameter stainless-steel vacuum chamber (cf. Fig. 2). The facility is supported by six 81-cm-diameter diffusion pumps each rated at 32,000 l/s (with water-cooled coldtraps), backed by two 2,000 cfm blowers, and four 400 cfm mechanical pumps. These pumps give the facility an overall pumping speed of over 100,000 l/s at 10^{-5} Torr. In addition, a Polycold PFC-1100 closed-loop water cryopump has been installed to double the water pumping speed of the facility (to over 150,000 l/s for H_2O). This, greatly reduces the pump-down time needed for the facility. It typically takes four hours to evacuate the chamber to 3×10^{-5} Torr from atmospheric pressure.

Chamber pressure is measured with MKS model 919 hot-cathode ionization gauges located on vacuum ports on either side of the chamber and by MKS Type 317HA Baratron capacitance manometers located in the center of the chamber (cf. Fig. 2). Background chamber pressure is maintained to less than 3.8×10^{-4} Torr (0.04 Pa) during arcjet operation on simulated hydrazine and to 1.5×10^{-4} Torr (0.01 Pa) while the arcjet operates on 15 mg/s (10 SLPM) of pure hydrogen.

Mixtures of nitrogen and hydrogen were used for all experiments to simulate hydrazine and ammonia decomposition products. For this study, the arcjet was operated at hydrogen flow rates of up to 16 mg/s and nitrogen flow rates of up to 41 mg/s. Propellant is supplied to the arcjet from compressed gas bottles through stainless-steel feed lines. The hydrogen bottles are stored in a shed outside of the laboratory. Hydrogen leak detectors are used to track hydrogen leaks through the propellant feed and vacuum exhaust systems. Nitrogen is injected into each of the mechanical pumps gas ballasts and exhaust manifolds to dilute the hydrogen prior to atmospheric exhaust.

Propellant flow is controlled and monitored with an array of MKS 1159B mass flow controllers specially calibrated for light and heavy gases. The system is capable of handling up to 16 mg/s of hydrogen and 110 mg/s of nitrogen with an accuracy of 1%. The flow controllers are periodically calibrated with a calibration rig that measures gas pressure and temperature changes, with time, in an evacuated chamber of know volume to estimate the mass flow rate (via the ideal gas law).

Thruster operation is visually monitored and stored with a Sony camcorder connected to a JVC Super VHS Cassette Recorder. A filter wheel is placed in front of the video camera to allow band-pass filtered images of the plume to be stored on film. Video frames are downloaded to and stored on a Macintosh computer (cf. Fig. 1) for image processing and analysis through the use of a frame grabbing system developed by Radius.

A Macintosh based data acquisition system, developed by National Instruments (LabVIEW) and controlled by

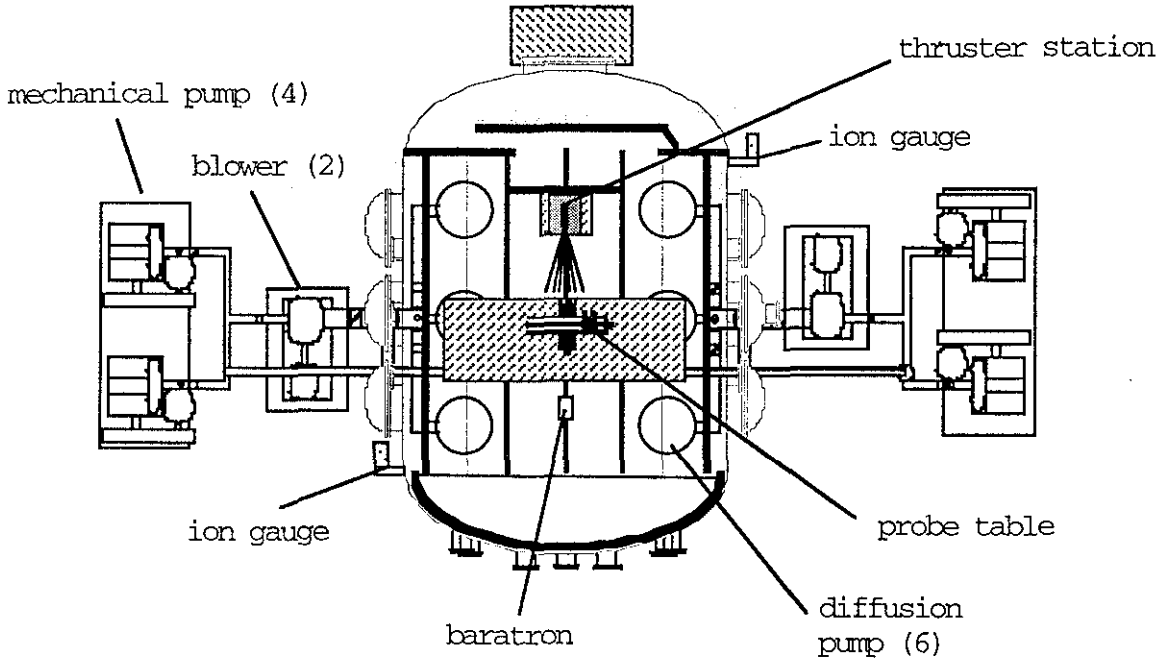

Figure 2: Schematic of the 9 by 6 meter vacuum chamber.

LABVIEW II, software, monitors all thruster, diagnostics, and tank operations. The system includes four SCXI-1120 8-channel isolation amplifiers that are used in conjunction with a NB-MIO-16XH-18 data acquisition board, and a NB-MIO-GPIB high-speed IEEE-488.2 interface card. This configuration provides thirty-two isolated differential input channels and the ability to control instruments with IEEE-488.2 communication ports.

Results and Discussion

The arcjet was allowed to run for a 20 minute warm-up period after ignition before measurements were made. This time was determined to be the duration needed for the arcjet to reach thermal equilibrium, on the basis of discharge voltage. Voltage and current ripple were measured with a four channel 500 MHz Tektronix TDS540 digital oscilloscope which is capable of collecting 50,000 pts at 250 million Samples/sec per channel. The oscilloscope traces are transferred to a computer via the National Instruments NB-MIO-GPIB board. At 10 A, 110 V, and 15 mg/s (10 SLPM) of H_2, current and voltage ripple were measured to be approximately 1.4 A and 6 V, respectively, at a frequency of 18 kHz, well within the nominal operating parameters of the PPU[9].

Performance Measurements

In an attempt to verify that the arcjet was operating properly, performance measurements were made with simulated N_2H_4 at 47 mg/s, simulated NH_3 at 38 mg/s, and pure H_2 at 15 mg/s. The thrust stand that was used is based on the inverted pendulum design used at NASA LeRC[10]. The arcjet was mounted to a Macor slab that is attached to an aluminum plate, which in turn, is connected to the base of the thrust stand through a series of stainless steel springs. The aluminum plate is connected to the core of a Lucas Schaevitz model 100-HR Linear Variable Differential Transformer (LVDT). The core resides within a LVDT coil that is mounted to the base of the thrust stand. The output from the LVDT is routed to a Lucas Schaevitz DTR-451 Digital Transducer Readout (DTR) that was been calibrated in its low sensitivity mode, and to the data acquisition system. Arcjet/thrust-stand leveling is performed manually prior to chamber pump-down so that the core is in its null position within the coil. In-situ thrust stand calibration is performed by loading and off-loading small weights to simulate thrust via a remotely-controlled stepper motor driven pulley system. A linear curve-fit of LVDT displacement vs. thrust is then obtained and used for performance measurements. Soon after the arcjet is turned off, a post-test calibration is performed. The springs of the stand were made with extra stiffness to minimize thruster

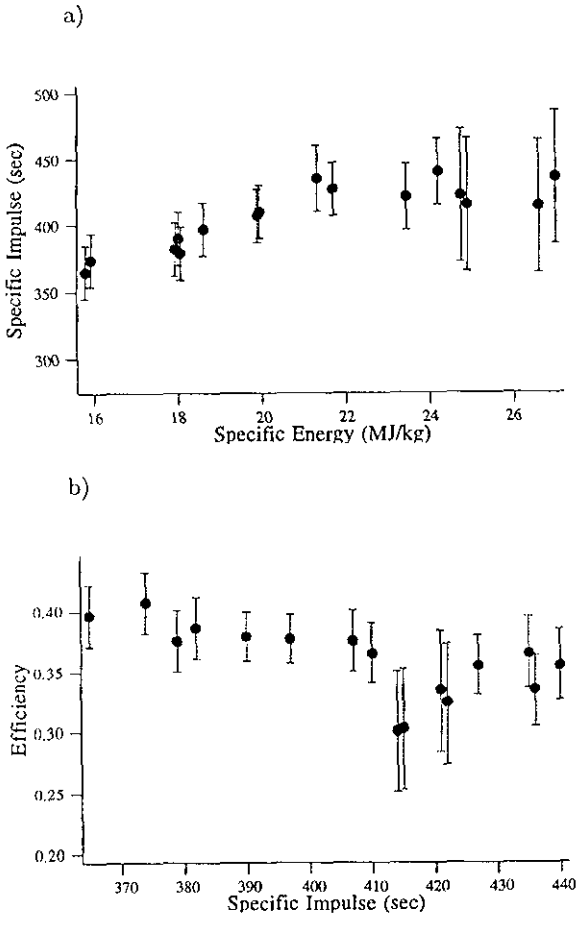

Figure 3: Arcjet performance data for simulated hydrazine ($\dot{m}$=47 mg/s).

deflection, thus allowing plume measurements to be made concurrently with thrust measurements.

Thrust data, based on the predetermined curve fit is displayed and simultaneously stored by the data acquisition system. The data acquisition system also reads mass flow rate, current, and voltage, enabling it to calculate thrust efficiency and specific impulse.

Because the facility does not yet have water handling capability, the entire inverted pendulum thrust stand is enclosed in a stainless-steel shell which sits on a movable platform. Pre-run and post-run calibration curve fits, which usually differ only in intercept, are used to account for thermal drifts, however, as the performance data below show, active cooling will have to be incorporated into the stand. Therefore, the stainless-steel shell will soon be replaced with a water-cooled copper shell.

Fig. 3 shows arcjet performance data for simulated hydrazine at 47 mg/s and for currents between 6 and 12 A; the entire range of the PPU. Thrust efficiency is calculated with the following equation:

Propellant	I_{sp} (sec)	Efficiency (%)
N_2H_4 (47 mg/s)	426	36
NH_3 (38 mg/s)	411	30
H_2 (15 mg/s)	700	32

Table 1: Summary of arcjet performance at 10 A.

$$\eta_{th} = \frac{{I_{sp}}^2}{(\frac{2}{g^2})(\frac{P_a}{\dot{m}})}. \quad (1)$$

This definition of thrust efficiency does not take into account cold-gas thruster performance, nor does it include corrections to I_{sp} for background pressure effects.

As the figure shows, thrust efficiency ranges between 30 and 40%, and specific impulse is between 350 and 450 sec. Since at low power levels (i.e., current below 10 A) the thrust and I_{sp} measurements are expected to be accurate to within a few percent, the smaller error bars on the figures represent the spread in raw data, typically 5%-7%. For currents above 10 A, thrust was measured to decrease with increasing power. This is obviously a result of excessive thermal drifts of the thrust-stand. Attempts at taking this drift into account after the arcjet was turned off were not successful since thermocouples attached to the stainless-steel shell showed that once the arcjet is turned off, the thrust stand quickly cools off; prior to the post-run calibration.

Although not shown on the figure, performance measurements with NH_3 and H_2 at 10 A and the mass flow rates noted above were also made. Typical values are presented in Table 1.

Near-field Measurements

All near and far-field arcjet measurements were made with the arcjet operating on pure hydrogen at a mass flow rate of 15 mg/s (10 SLPM), and at a current of 10 A. A typical chamber pressure for this operating condition was 1.5×10^{-4} Torr.

Plume diagnostics, both in the near and far fields, were performed through the use of a custom-made probe positioning system developed by New England Affiliated Technologies (NEAT). The table contains two rotary platforms on a 1.8-m-long (6 ft) linear stage in the radial direction that is mounted on a 0.9 m (3 ft) travel axial stage. The rotary actuators not only allow Langmuir and pressure probes to be rotated to minimize measurement errors due to probe misalignment with the flow[11, 12, 13, 14], but also for the purpose of characterizing the local flow field. The system allows for sweeps with two probe rakes at a time at radial speeds in excess of 60 cm/s with an absolute position accuracy of 0.15 mm with time (or position) varying probe angles. The system

is operated by its own Macintosh-driven control station via LABVIEW II software. Like the thruster station, the entire probe positioning system is mounted on a movable platform to allow for measurements to be made throughout the chamber (cf. Fig. 2).

Near-Field Langmuir Probe Measurements

A cylindrical single Langmuir probe was used to measure n_e and kT_e near the exit of the arcjet. The probe is composed of a tungsten wire electrode, 0.23 mm (9 mils) in diameter and 1.9 cm (0.75 inches) long, attached to the center conductor of a triaxial boom that is constructed of titanium with Teflon insulation. The boom is approximately 4 mm in diameter and 18 cm long.

The collector electrode of the probe was biased with respect to the chamber wall by a Kepco model BOP 100-2M programmable bi-polar power supply which can provide an output voltage of ±100 V at up to 4.8 A. A function generator was used to provide the 12.7 Hz triangular source waveform that was amplified to ±10 V by bi-polar supply. Since the arcjet anode is tied to chamber ground, there is no need to use an isolated transformer for the bi-polar power supply.

Probe current, measured through a 10 Ohm shunt, and probe voltage, measured with respect to tank ground, were collected with voltage probes and operation amplifiers. Amplifier output signals were collected both by the data acquisition system for storage and later processing, and by the digital oscilloscope for real-time processing. The data acquisition system stored 50 pairs of probe voltage-current per voltage ramp.

All near-field measurements were made with the tip of the Langmuir probe placed 20 mm downstream of the nozzle exit. To collect data this close to the exit, the probe was quickly moved to the collection site (at the appropriate angle), kept there long enough to collect ten ramps of data (~1 sec), and rapidly move out of the plume to allow for probe cooling. This approach also served as an effective means of cleaning the probe.

Since in the near-field $r_p/\lambda_D \geq 10$ and $\lambda_i/r_p > 100$, the standard collisionless thin sheath Bohm ion saturation current model was used to interpret Langmuir probe data. To account for ion current collection due to convection from the flowing plasma, the probe angle was varied between 0 and 10 degrees with respect to the plume axis of symmetry. 10 degrees was determined to be the maximum angle possible for the boom of the probe not to perturb the flow.

Fig. 4 shows radial electron temperature and number density profiles. As the figure shows, electron number density measurements are quite sensitive to to probe angle. The peak value of n_e (slightly offset from the axis) at 10 degrees is more than twice that with the probe aligned with the thruster axis. However, the n_e data for the three probe orientations converge with increasing radius, and identical values are predicted 18 mm from the centerline.

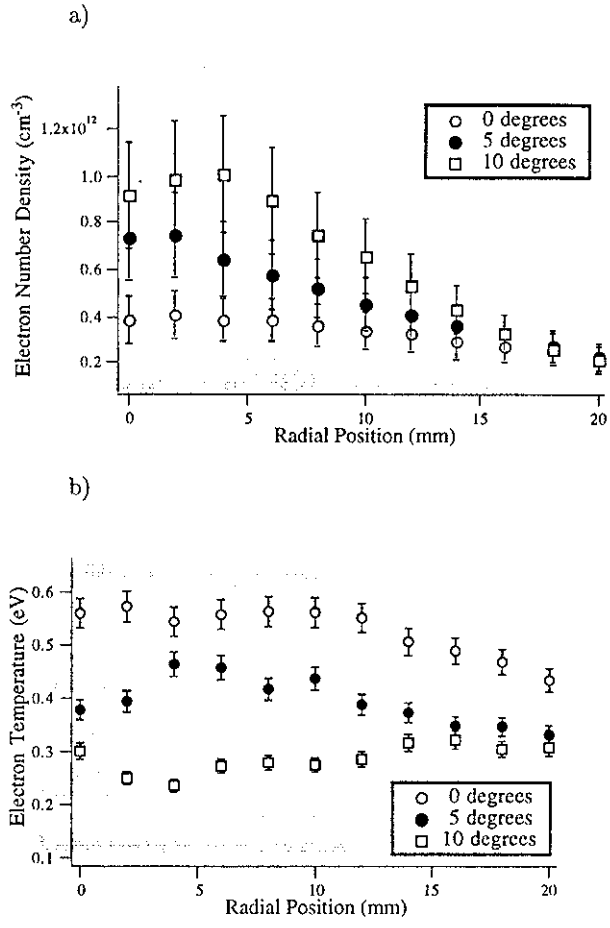

Figure 4: Electron number density and temperature profiles.

LIF measurements have shown the axial velocity of hydrogen arcjets to decrease rapidly with radius[15]. Thus, the fact that probe angle has little influence on number density measurements at this location may be an indication that the local flow velocity is close to the heavy particle thermal speed, and so convective ion collection at the probe becomes indistinguishable from random flux collection.

Higher than expected electron temperatures were measured with the Langmuir probe. Electron temperature is seen to decrease with increasing probe angle but to remain relatively constant with radius. This last trend has been observed in higher powered hydrogen arcjets (10 kW) via emission spectroscopy[16]. Only the 0 degree probe data predict expected values of kT_e. The reason for this probe angle dependence is not known at this time.

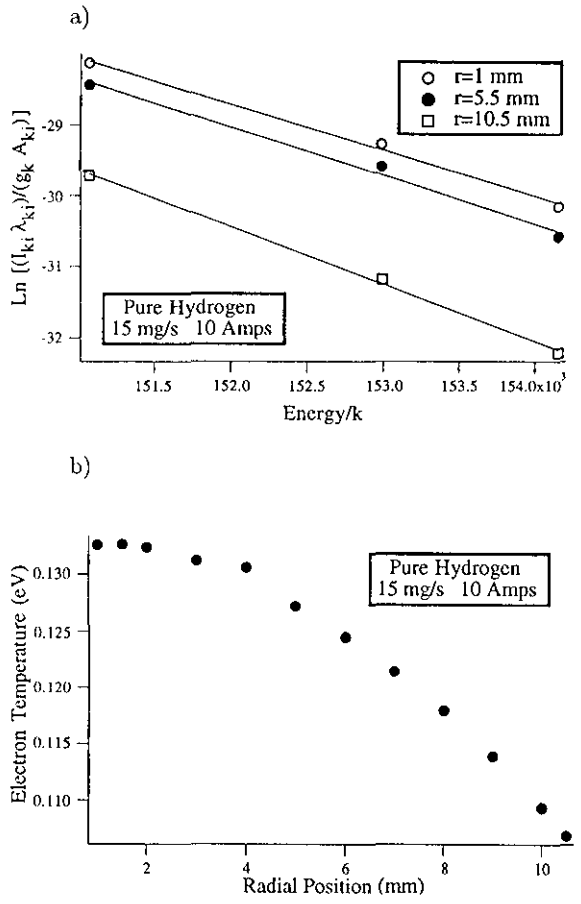

Figure 5: Boltzmann plot of excited states, and corresponding Electron temperature vs. radius profile with H_2 propellant.

Emission Spectroscopy

Spectroscopic measurements were made with a Spex Industries model 500M Czerny-Turner type spectrometer. The spectrometer has a focal length of 0.5 meters, an f/4 aperture, and a dual exit assembly to allow for the installation of both a Photo Diode Array and a Photo Multiplier Tube. A 1800 gr/mm holographic grating, blazed at 500 nm, was used for all measurements, giving the spectrometer a dispersion of 1.2 nm/mm, a spectral range between 120-1000 nm, and a wavelength resolution of 0.015 nm. Light detection is achieved using a Hamamatsu R928 photomultiplier tube powered by a Spex-35870-1 high voltage power supply. High voltage to the tube is computer controlled via the Spex Datascan unit. Spectrometer scans are monitored, controlled, and stored on a Gateway 2000 486 personal computer (PC) through Spex Industries' Autoscan software. A Stanford Research SR850 Dual Phase Analog Lock-in Amplifier, in conjunction with a chopper, was sometimes used to provide phase-locked spectrometer scans.

Because of the large size of the chamber, direct optical access to the exit of the thruster is difficult to achieve. Thus, light from the arcjet plume is focused onto the face of a 100-micron-diam. silica optical fiber by a 25-mm-diam. achromatic lens within the chamber, and is transmitted to the spectrometer via a vacuum feedthrough. The exiting light from the optical fiber is then focused onto the entrance slit of the spectrometer by another achromatic lens.

Characterization of the spectral response for this imaging system was made using a tungsten lamp as a light source in place of the arcjet plume. Emissivity values for tungsten were used to determine the actual spectral output of the lamp. True lamp intensity along with corresponding measured intensity acquired from the spectrometer photomultiplier tube signal was then used to determine the system's spectral response. The spectral response function was used to correct the measured intensity at a given wavelength to its true value.

In order to allow radial scans to be made at or near the arcjet exit plane, the collection optics are mounted on a NEAT 28 cm (11 inch) linear positioning table that is vertically mounted to the side of the thruster station next to the thrust stand. This allows the collection optics to be position approximately 10 cm above or below the center of the plume. When not in use, the collection lens is stored in a "safe-box" at the top of the stage. The table is controlled by a PC.

All spectra were taken with the arcjet operating at 10 A at a mass flow rate of 15 mg/s of pure hydrogen. The arcjet is allowed approximately 20 minutes to reach equilibrium before spectra are taken. Data were taken by translating the optics in 1 millimeter increments perpendicular to the plume axis 12 mm downstream of the exit plane and 15 cm to the side of the arcjet centerline. The spectrometer entrance slit was set at 100 microns to maximize the amount of light collected by the spectrometer while the exit slit was set at 500 microns to ensure capture of Stark broadened hydrogen lines. The emissivity coefficient for each measured transition was then calculated from intensity profiles along various chords of the plume via Abel inversion. With the emissivity coefficient, Boltzmann plots were then made to determine the electron temperature as a function of radius.

Fig. 5 a) shows examples of Boltzmann plots made at three radial locations, 12 mm downstream of the exit plane. The 434 nm, 410 nm, and the 397 nm hydrogen lines hydrogen Balmer lines were used for this plot. The linearity of this plot suggests that the upper states used in the Boltzmann plot are in local thermal equilibrium with the electrons and can be used to measure electron temperature.

Fig. 5 b) plots electron temperature, as is determined from the Boltzmann plot, as a function of radial position. As the figure shows, the electron temperature drops off rapidly with radius. The peak electron temperature

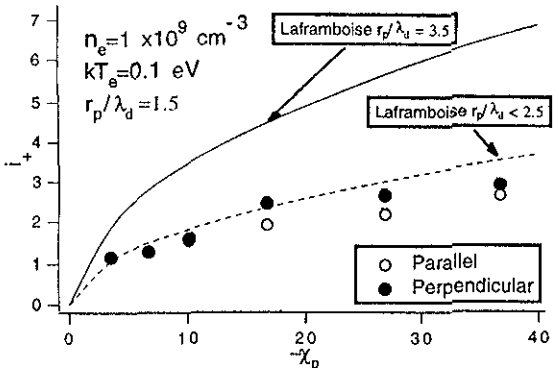

Figure 6: Normalized ion current vs. probe potential.

of ~0.13 eV is found near the center of the plume. At 10.5 mm from the plume center, the electron temperature drops to less than 0.11 eV. Initially, four hydrogen Balmer lines were used in this study for making Boltzmann plots; the 486 nm, 434 nm, 410 nm, and the 397 nm hydrogen lines. It was observed, however, that the electron temperatures predicted with these Boltzmann plots increased with radius, a trend which is counterintuitive. This behavior suggests that the low lying states on the plot may not be in equilibrium with the electron energy distribution.

The 486 nm state lies 0.31 eV below the nearest upper exited state in the Balmer series. As a consequence of the wide (relative to kT_e) energy spacing between this state and its nearest upper excited state, it is improbable that the electrons are in equilibrium with it. Additionally, the intensity of this state decreases with radius as the true electron temperature and density decreases, and as the lower lying excited states in general fall further out of equilibrium. This results in a flattening of the slope of the Boltzmann line at large radii, resulting in artificially high kT_e. This low lying state was thus removed to make Fig. 5 a), and the data were refitted to predict the electron temperature profile shown in Fig. 5 b). The electron temperatures calculated from the the corrected Boltzmann plot are consistent with the energy spacing between these upper states. This finding suggests that the upper states used in Fig. 5 a) are in local thermal equilibrium with the electrons and can be used to measure electron temperature. Of concern is the disagreement between Langmuir probe and spectroscopy kT_e data. Unfortunately, time did not permit for a thorough investigation into the source of this discrepancy to be made at present.

Far-field Measurements

Far-field Langmuir Probe Measurements

In order to measure electron temperatures and densities approximately one meter from the arcjet exit plane, where λ_D is on the order of 0.1 mm[7], a 0.42-cm-diameter by 5.1-cm-long rhenium cylindrical Langmuir probe was used in conjunction with the smaller probe that was used for near-field single-probe measurements. The collector electrode was formed by vapor-depositing rhenium on a molybdenum mandrill.

In the far-field, λ_e and λ_i are expected to be an order of magnitude larger than the diameter of the large probe and at least two orders of magnitude larger than the sheath. Furthermore, since r_p/λ_D will be approximately 20 or more for the large probe, a thin sheath saturation current model was used to analyze data from large probe.

To interpret data from the small probe in the far-field, where $r_p/\lambda_D \simeq 1$, a current saturation model from Laframboise was used[17]. This model is accurate for cylindrical Langmuir probes in quiescent plasmas devoid of magnetic fields where $r_p/\lambda_D < 2.5$,[17]:

$$I_+{}^2 = (2e^3 n_e{}^2 A^2/\pi^2)(Z_i/M_i)(\Phi_p - V). \quad (2)$$

It should be noted that in contrast to the Bohm thin sheath model, in this limit ion saturation current no longer depends on electron temperature.

To test the validity of the model, the ion saturation current of the small probe was measured as a function of probe potential while it was kept in a portion of the arcjet plume where the electron temperature and number density had been measured at ~0.1 eV and 1×10^9 cm^{-3}, respectively, by the large probe. The probe was placed along the center of the plume both parallel and perpendicular to the axis of the arcjet. This data is shown on Fig. 6 which plots dimensionless ion saturation current, defined by the following equation:

$$i_+ = I_+/(en_e A(Z_i kT_e/(2\pi \mathrm{M_i}))^{1/2}), \quad (3)$$

versus dimensionless probe potential:

$$\chi_P = e(V - \Phi_p)/kT_e. \quad (4)$$

Also plotted are Laframboise's models for $r_p/\lambda_D < 2.5$ (Eqn. 2) and for $r_p/\lambda_D = 3.5$[17]. As the figure shows, Laframboise's models for the case of $r_p/\lambda_D < 2.5$ is in excellent agreement with the small probe data, where $r_p/\lambda_D \simeq 1.5$. The figure also shows that slightly higher saturation currents are measured when the probe is perpendicular to the local ion flow, as is expected.

Fig. 7 shows profiles of electron temperature and number density as measured with the large probe using the thin sheath model. The probe angle was rotated to 0, 5, 10, 20, and 30 degrees with respect to the thruster axis at each location. The table position was adjusted automatically at each angle to ensure that the collector electrode of the probe was in the appropriate axial and radial positions. The probe was moved continuously at a radial speed of 1.2 cm/s. Thus, 50 pairs of probe

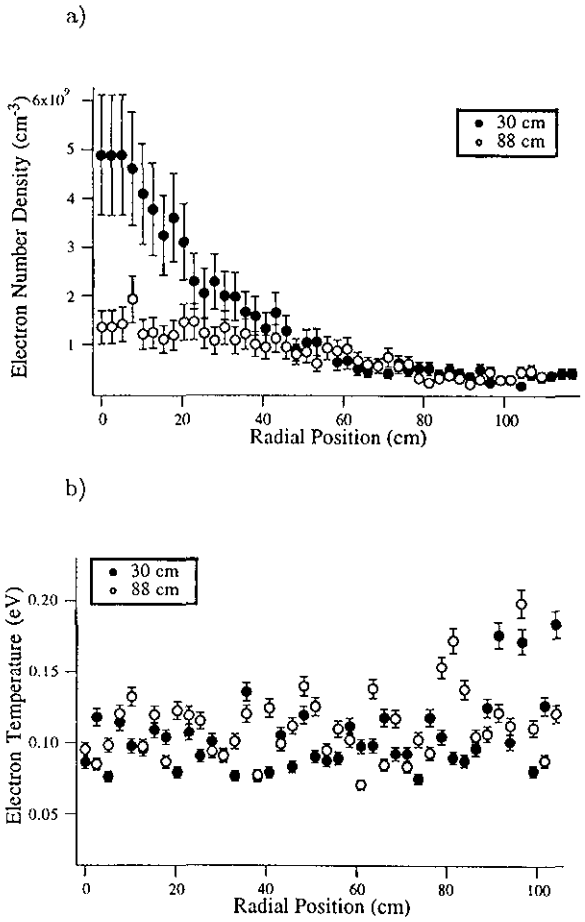

Figure 7: Electron number density and temperature profiles.

voltage-current data points were collected per millimeter of radial travel (voltage ramp). A Hewlett-Packard workstation running MATLAB was used to process the tens of thousands of data points to obtain electron temperatures and number densities. Only data collected at angles at which the axis of the probe is aligned with the local flow (i.e., minimum ion saturation current) are reported.

As the figure shows, the peak number density drops from 5×10^9 to less than 2×10^9 cm^{-3} over a half-meter increase in axial position. At 30 cm from the exit, the number density at the edge of the measurement region is nearly an order of magnitude smaller than the peak value. At the 88 cm position, the radial electron number density profile is flat, suggesting that the exhaust rapidly assumes a uniform spherical expansion pattern. The variation in electron temperature, however, is not so nearly dramatic, and is approximately 0.1 eV at both axial locations. The increased scatter and indicated temperature at the fringe of the measurement region may be due to probe misalignment with the flow.

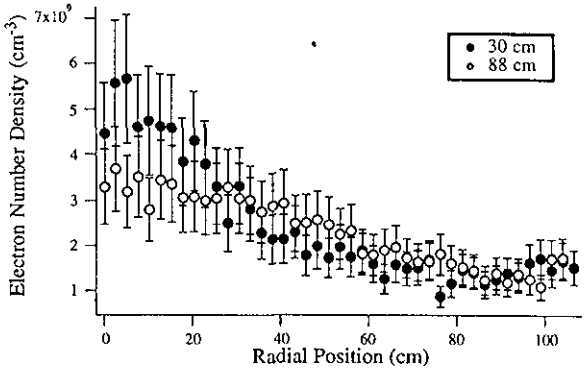

Figure 8: Electron temperature and number density profiles.

Partially corrected number density data from the small probe are plotted on Fig. 8. The partial correction made to the data includes using electron temperature data obtained with the large probe with a Bohm model. This adjustment was necessary since kT_e values calculated from the small probe assuming Bohm current collection were approximately an order or magnitude too high ($\sim$1 eV). Although the source of this error is thought to be due to the erroneous model used, no attempt was made to incorporate Laframboise's models in calculating T_e or n_e with the small probe at this time. The fact that the peak number density in Fig. 8 is slightly offset from the 0 cm radial position may be an indication that the probe axis is slightly misaligned with the thruster centerline.

Using the Bohm model, the data from the small probe tend to be flatter in profile than those from the large probe, and tend to over-predict n_e throughout the plume. The overprediction in n_e at the region of the plume of lowest density is expected since the probe finite sheath thickness effects are expected to have a significant effect on current collection. In fact, this phenomenon can be exploited as a diagnostic. By using the electron temperatures and number densities measured with the large probe in conjunction with the saturation currents measured with the small probe, an estimate of the sheath thickness can be made (i.e., by calculating the effective collection area of the small probe). Preliminary calculations to this effect have found that the effective collection area of the small probe is approximately 2.5 times that of the actual probe surface, in the case of $r_p/\lambda_D \simeq 1.5$. This suggests that the radius of the collection cylinder is $\sqrt{2.5}$ times r_p, and that the sheath thickness is $0.6r_p$. Since, $\lambda_D/r_p \simeq 1/1.5 = 0.67$, the sheath that forms on the small probe is approximately one Debye length thick.

Electron number density data from the large probe were compared to data obtained from a microwave interferometer described in Ref. [18]. As the figure shows,

a) 30 cm

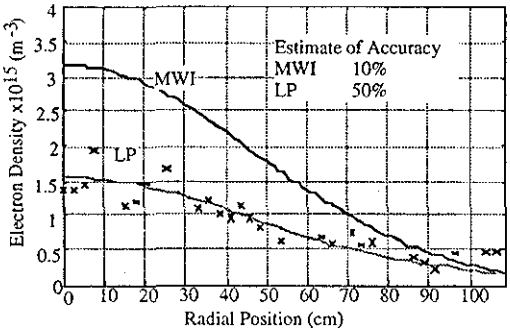

b) 88 cm

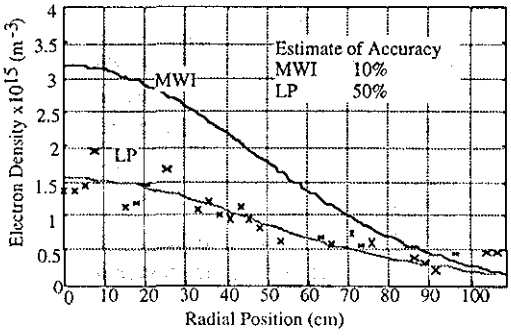

Figure 9: Comparison of number density profiles obtained from Langmuir probes and through microwave interferometry at two axial locations [Ref. 18].

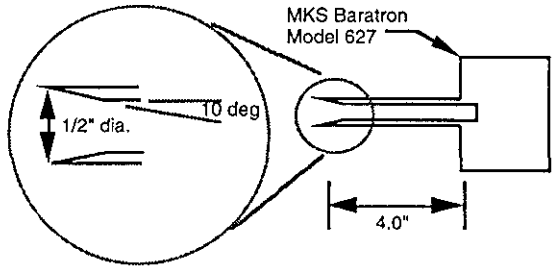

Figure 10: Detail of the impact pressure probe assembly showing 10 degree internal chamfer on probe lip.

electron number densities predicted by the interferometer are consistently larger than those obtained from the large Langmuir probe. Given the inherently superior accuracy of n_e measurements from the microwave interferometer in comparison to the Langmuir probe (i.e., 10% vs. 50%), it is anticipated that the interferometry data shows true number densities and that the Langmuir probe artificially suppresses n_e. Although this trend has been observed recently in other studies in which the probe was thought significantly perturb the local charge density in a radio-frequency discharge[19], no conclusive explanation can be given for our results at this time.

Plume Pressure Measurements

The task of measuring plume pressures in a supersonic rarefied flow represents several challenges. In flows with Knudsen numbers of order one (transitional flows), particle interactions with the probe structure, in terms of heat transfer and scattering, can profoundly affect measured pressures[20, 21, 22, 23, 24]. These non-equilibrium effects often render pressure data from poorly designed pressure probes useless. To investigate this effect, an impact probe was designed and placed in the far-field plume of the arcjet operating on 15 mg/s of hydrogen at 10 A. The probe consists of a 10-cm-long by 1.3-cm-diameter (o.d.) aluminum tube, with a 10 degree lip, attached to an MKS model 627 Baratron capacitance manometer that was calibrated to a pressure of 1×10^{-4} Torr. The purpose of the chamfer is to minimized edge effects at the collection orifice[14].

Output from the Baratron was processed with an MKS PDR-C-1C display and the LabVIEW data acquisition system (cf. Fig. 10). The probe assembly was connected to a boom that was placed on the probe positioning system. Through use of the theta table, the probe could be rotated to more than ± 90 degrees from the thruster axis.

Fig. 11 shows typical data from a theta scan from -90 to 90 degree, with the probe at a fixed spatial location approximately 0.5 meters from the nozzle exit. The local flow angle can be interpreted as the point corresponding

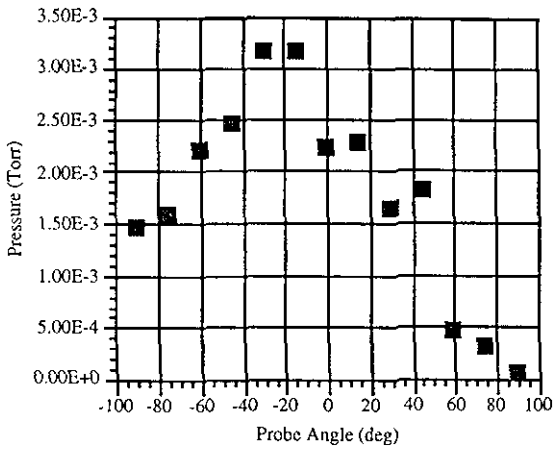

Figure 11: Impact probe pressure vs. probe angle for data taken 47.6 cm downstream of the exit plane and 25.4 cm radially from the plume center.

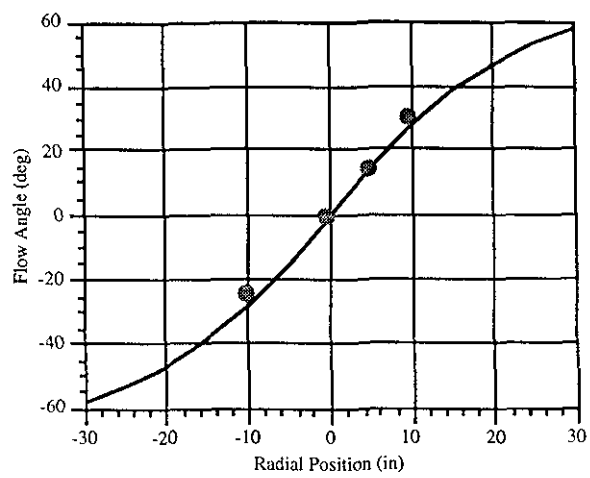

Figure 12: Flow angle, as determined from impact probe measurements, vs. radial position 25 cm downstream of the nozzle exit.

to the maximum pressure reading (i.e., when the probe is pointed directly into the oncoming flow). The figure shows that the local flow angle at this spot is approximately 20 degrees with respect to the thruster axis. This process can be repeated at various axial and radial locations to map the local flow field in terms of direction. An example of this is shown in Fig. 12 which shows flow angle as a function of radial position 48 cm downstream of nozzle exit. Flow angle at each spot is determined from recording the angle of maximum pressure when the probe is rotated through 180 degrees at a fixed spatial location. The curve on this figure shows flow angle as computed from the source flow model described below. As is expected, the flow angle of the expanding plume increases with radial position. Although few points are reported, the fact that the data corroborate the source flow code and are symmetric about the thruster centerline (0 inch position) is especially encouraging.

Although it has been demonstrated that this technique can be used to qualitatively map the far-field flow pattern, it was of particular interest to determine if absolute pressure measurements could be made. To this effect, the Revised Plume Model code (RPM) from the NASA-Johnson Space Center (JSC) was used to generate dynamic pressure simulations for the arcjet. The code is capable of generating a complete spatial flowfield map of dynamic pressure values for a nozzle exhausting into vacuum. The input parameters for the code include nozzle geometry, stagnation pressure and temperature, molecular weight, γ, and the boundary layer thickness at the nozzle exit.

The RPM code was written by NASA-JSC with the goal of obtaining an accurate model of the Shuttle Orbiter's Primary Reaction Control System (PRCS) nozzle plumes[25]. The code has been ground verified and modified using conventional cold gas expansion nozzles in a large vacuum chamber. No attempt was made to extend the code to plumes produced by arcjets or any other type of electric propulsion device. The motivation behind the use of RPM in this research was to test the validity of this model in the mid to far field region of a 1 kW arcjet plume and to use it for comparison against impact pressure probe data.

Since the ionization fraction of the plume is low ($< 10^{-2}$), a high temperature neutral gas (30% dissociated hydrogen) was assumed for the model. Thus, the very small amount of ionization in the plume combined with the simple nozzle geometry will create a plume flow field that is similar to that of a conventional rocket with a high exhaust temperature[26]. Successful extension of conventional plume flow field solvers such as RPM to the plume of arcjets provides a simple method of predicting the flow of the neutral species from these devices. This application, if successful, would eliminate the need for development of costly arcjet solvers employing complicated (and unnecessary) models to account for ionization and dissociation in the plume.

The RPM code is based on a source flow model; the source flow model assumes that the neutral gas species behaves as if it were emitted from a supersonic point source located at the nozzle exit plane. The density of this flow is assumed to fall off as the radius squared in the inviscid core of the plume to satisfy mass conservation. An exponential decay factor is applied to the gas originating from the nozzle boundary layer. The funda-

mental underlying equation of the model is given below for dynamic pressure, q,

$$q = A_o P_b \frac{A^*}{A_e} \left(\frac{r_e}{r}\right)^2 \frac{\gamma}{\gamma - 1} \left(\frac{2}{\gamma + 1}\right)^{\frac{1}{\gamma - 1}} \xi(\theta). \quad (5)$$

For $\theta < \theta_o$

$$\xi(\theta) = \left[\cos\left(\frac{\pi}{2} \frac{\theta}{\theta_L}\right)\right]^{\frac{2}{\gamma - 1}}. \quad (6)$$

For $\theta_o \leq \theta \leq \pi$,

$$\xi(\theta) = \left[\cos\left(\frac{\pi}{2} \frac{\theta}{\theta_L}\right)\right]^{\frac{2}{\gamma - 1}} e^{-(\beta + 2\chi)(\theta - \theta_o)}. \quad (7)$$

The parameter θ_o is defined as the angle where the inviscid plume core meets the boundary layer gas in the nozzle, θ_L is the limiting Prandtl-Meyer expansion angle, and the parameters β and χ are related to the density and velocity decay in the nozzle boundary layer flow[26]. A_o and P_b are parameters related to the formation of the boundary layer and the supersonic expansion of the flow outside of the nozzle[27]. This model is expected to be most accurate within 60 degrees of the thruster axis.

Fig. 13 shows comparisons between dynamic pressure profiles predicted by the code and impact pressure probe data at two axial locations (53 and 64 cm from the nozzle exit). As model inputs, the arcjet boundary layer thickness was estimated to be 1 mm at the exit, and the total bulk temperature and pressure were set at 3300°K and 0.27 MPa, respectively. Data points represent radial sweeps at discrete probe angles across the entire radial table (60 inches long) within a 50 degree cone from the nozzle. As the figure shows, at each axial location the envelope of data is enclosed in the profile predicted by the model. The model predicts higher pressures near the ends of the table (±30 in) than are measured. For these measurements, tank pressure was recorded at 1.4×10^{-4} Torr with the side-mounted ionization gauges (cf. Fig 2). Thus, the fact that dynamic and static pressure at the edge of the measurement region falls below the lower limit detectable by the Baratron (10^-4 Torr) not only corroborates ionization gauge data, but suggests that the bulk of the neutrals flows within a 2-m-diam. region at these axial locations. Lastly, by comparing measured pressures with measured electron temperatures and number densities at these axial positions, and by assuming a heavy particle translational temperature of 2000°K, an upper limit to the on-axis neutral gas density was calculated to be $\sim 10^{13}$ cm^{-3}, corresponding to an ionization fraction of $\sim 10^{-4}$.

a) 53 cm

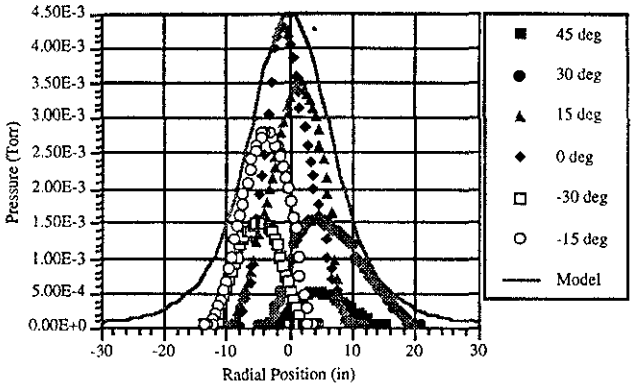

b) 64 cm

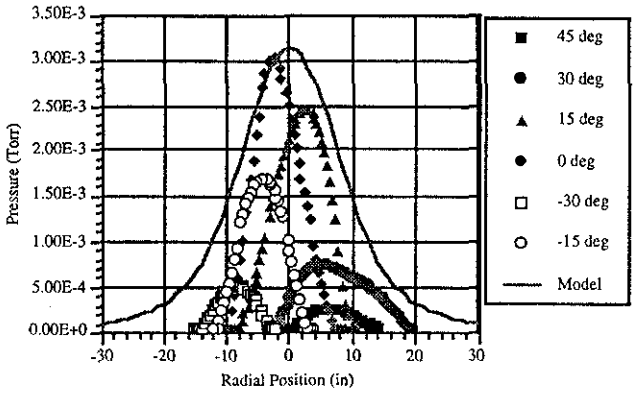

Figure 13: Impact pressure probe data at various angles vs. radial position at axial positions 53 and 64 cm from the nozzle exit.

Conclusions

A detailed study of the plume from a 1 kW hydrogen arcjet has been performed. Langmuir probe, impact pressure probe, emission spectroscopy, and microwave interferometry were all employed in this study (also see Ref. [18]). In the near-field region, analysis of the hydrogen Balmer lines suggests that only the upper states of that series are in local thermodynamic equilibrium with the electrons, and use of lower states could result in erroneous temperature measurements. Near-field Langmuir probe measurements at varying probe angles suggest that the axial flow velocity 20 mm downstream of the nozzle exit varies rapidly with radius and at 20 mm from the centerline, the exhaust plume may be near the local heavy particle thermal speed.

The Langmuir probe was found to accurately predict far-field number densities (according to microwave interferometric data of Ref [18]) using the Bohm saturation model when its radius is much larger than the local Debye length. An ion saturation current model from Laframboise was found to accurately account for finite sheath effects that are present when the probe dimensions are on the order of the Debye length. By using saturation

current data from two probes of different sizes, it was concluded that the sheath thickness in the plume is approximately 1 Debye length.

Comparison of impact pressure probe measurements with a source flow model was favorable. It was demonstrated that flow field information could be obtained from these measurements and that a relatively simple instrument could be used to measure dynamic pressure. By incorporating measured electron temperatures, number densities, and an assumed heavy particle temperature with these pressure data, the ionization fraction was estimated to be 10^{-3} or less.

Acknowledgments

The authors would like to thank Shawn Ohler for help in analyzing far-field data, Colleen Marrese for general "VI" development, and Mark Reichenbacher for writing software sequences for the probe positioning system. The authors would also like to thank the technical support staff of the Aerospace Engineering Department for their help in maintaining the facilities, NASA LeRC and JSC for instrumentation support and advice, Arnaud Turlan for data processing, and Dr. Larry Brace of the University of Michigan's Space Physics Research Laboratory for use of his Langmuir probes.

This work was supported through grants from NASA LeRC and BMDO (Dr. Frank Curran - contract monitor), from NASA JSC (Mr. Ricardo Machin - contract monitor), and the University of Michigan Office of the Vice President for Research.

References

[1] Smith, R. D., Yano, S. E., Lichtin, D. A., and Beck, J. W., "Flight Qualification of a 1.8 kW Hydrazine Arcjet System," IEPC-93-007, 23^{rd} *Internatinal Electic Propulsion Conference*, Seattle, WA, Sept. 13–18, 1993.

[2] Sneegas, S. A., Rosenthatl, R. A., Vondra, R. J., "Space Surveillance Trank and Autonomous Reposition (SSTAR) Experiment," IEPC-93-054, 23^{rd} *Internatinal Electic Propulsion Conference*, Seattle, WA, Sept. 13–18, 1993.

[3] Sutton, A. M., "Overview of the Air Force ESEX Flight Experiment," IEPC-93-057, 23^{rd} *Internatinal Electic Propulsion Conference*, Seattle, WA, Sept. 13–18, 1993.

[4] Sankovic J. M., Hamley, J. A., Haag T. W., and Curran F. M., "Hydrogen Arcjet Technology," IEPC-91-018, (NASA TM-105340), 22^{nd} *International Electric Propulsion Conference*, Viareggio, Italy, Oct. 14–17, 1991.

[5] Curran F. M., Bullock, S. R., Haag T. W., Sarmiento, C. J., and Sankovic J. M., "Medium Power Hydrogen Arcjet Performance," AIAA-91-2227, (NASA TM-104533),27^{th} *Joint Propulsion Conference*, Sacramento, California, June 24–27, 1991.

[6] Pivirotto, T., King, D., Deninger, W., and Brophy, J., "The Design and Operating Characteristics of a 30 kW Thermal Arcjet Engine for Space Propulsion," AIAA-86-1508, 22^{nd} *Joint Propulsion Conference*, Huntsville, Alabama, June 16–18,1986.

[7] Carney, L. M., and Sankovic, J. M., "The Effects of Arcjet Thruster Operating Conditions and Constrictor Geometry on the Plasma Plume," AIAA-89-2723, (NASA TM-102285), 25^{th} *Joint Propulsion Conference*, Monterey, California, July 10–12, 1989.

[8] Pencil, E. J., Sarmiento, C. J., Lichtin, D. A., Palchefsky, J. W., and Bogorad, A. L., "Low Power Arcjet System Spacecraft Impacts," AIAA-93-2392, 29^{th} *Joint Propulsion Conference*, Monterey, California, June 28–30, 1993.

[9] Gruber, R. P., "Power Electronics for a 1-Kilowatt Arcjet Thruster," AIAA-86-1507, (NASA TM-87340),22^{nd} *Joint Propulsion Conference*, Huntsville, Alabama, June 16–18,1986.

[10] Haag T. W., and Curran F. M., "Arcjet Starting Reliability: A Multistart Test on Hydrogen/Nitrogen Mixtures," AIAA-87-1061, (NASA TM-898867), May, 1987.

[11] Tilley, D. L., Gallimore, A. D., Kelly, A. J., and Jahn, R. G., "The Adverse Effect of Ion Drift Velocity Perpendicular to a Cylindrical Triple Probe," Review of Scientific Instruments (AIP) Vol. 65, No. 3 March, 1994.

[12] Steckelmacher, W., and Lucas, M. W., "Gas Flow through a Cylindrical Tube Under Free Molecular Conditions," J. Phys. D: Appl. Phys., Vol. 16, (1983) 1453-1460.

[13] Meyer, J. T., "Free Molecular Pressure Measurements in the Continuum, Transitional, and Free Molecular Regimes of a Free Jet," *Rarefied Gas Dynamics,* 17_{th} *Symposium*, 1990, pp. 963-970.

[14] Koppenwallner, G., "The Free Molecular Pressure Probe with Finite Length Slot Orifice," *Rarefied Gas Dynamics,* 14_{th} *Symposium*, 1984, pp. 415-422.

[15] Liebeskind, J. G., Hanson, R. K., and Cappelli M. A., "Flow Diagnostics of an Arcjet Using Laser-Induced Fluorescence," AIAA-92-3243, 28^{th} *Joint Propulsion Conference*, Nashville, TN, July 6–8, 1992.

[16] Hoskins, W. A., "Measurement of Population and Temperature Profiles in an Arcjet Plume," AIAA-92-3240, 28^{th} *Joint Propulsion Conference*, Nashville, TN, July 6–8, 1992.

[17] Laframboise, J., "Theory of Cylindrical and Spherical Probes in a Collisionless Plasma at Rest," Rarefied Gas Dynamics, Vol. 2, edited by J.H. deLeeuw, Academic Press, NY, 1966, pp. 22-44.

[18] Ohler, S., Gilchrist, B., and Gallimore, A. D., "Non-intrusive Electron Number Density Measurements in the Plume of a 1 kW Arcjet Using a Modern Microwave Inteferometer," AIAA-94-3297, Joint Propulsion Conference, Indianapolis, IN, June 27–29 1994.

[19] Overzet, L. H.,and Hopkins, M. B., "Comparison of Electron-density Measurements made using a Langmuir Probe and Microwave Interferometry in the Gaseous Electronics Conference Reference Reactor," J. Appl. Phys., 74, (7), 4323-4330, 1993.

[20] Wainwright, J.B., and Rogers, K.W. (1964). "Impact Pressure Probe Response Characteristics in High Speed Flows with Transition Knudsen Numbers." University of California Eng. College Report 101-101.

[21] Potter, J.L., Kinslow, M., and Boylan, D.E. (1964). "An Influence of the Orifice on Measured Pressures in Rarefied Flow." Arnold Eng. Develop. Center Tech. Doc. Rept.

[22] Hughes, P.C. (1965). "Theory for the Free Molecule Impact Probe at an Arbitrary Angle of Attack." University of Toronto Institute for Aerospace Studies Report No. 103.

[23] deLeeuw, J.M., and Rothe, D.E. (1962). "A Numerical Solution for the Free Molecule Impact Pressure Probe Relations for Tubes of Arbitrary Length." University of Toronto Institute for Aerospace Studies Report No. 88.

[24] Pond, M.L. (1962). J. Aero/Space Sci. 29, 917-920.

[25] Fitzgerald, S. M., Bouslog, S. A., and Hughes, J. R., "Model for Predicting Orbiter PRCS Plume Impingement Loads," NASA Document No. JSC-26507, Jan., 1994.

[26] Simons, G. A., "Effect of Nozzle Boundary Layers on Rocket Exhaust Plumes," AIAA Journal, Vol. 10, Nov., 1972, pp. 1534-1535.

[27] Bird, G. A., "Breakdown of Continuum Flow in Freejets and Rocket Plumes," Rarefied Gas Dynamics. Part II. Progress in Astronautics and Acronautics, Vol. 74.